







Article

Two Isomers of a Novel Ag(I) Complex with Pyrazole-Type Ligand—Synthesis, Structural, Thermal, and Antioxidative Characterization

Nikola D. Radnović ¹, Nađa Štetin ^{1,2}, Mirjana M. Radanović ¹, Ivana Đ. Borišev ¹, Marko V. Rodić ¹,
Željko K. Jaćimović ³ and Berta Barta Holló ^{1,*}

¹ Faculty of Sciences, University of Novi Sad, 21000 Novi Sad, Serbia; nikola.radnovic@dh.uns.ac.rs (N.D.R.); stetin.nadja@gmail.com (N.Š.); mirjana.lalovic@dh.uns.ac.rs (M.M.R.); ivana.borisev@dh.uns.ac.rs (I.Đ.B.); marko.rodic@dh.uns.ac.rs (M.V.R.)

² Telix d.o.o., 21000 Novi Sad, Serbia

³ Faculty of Metallurgy and Technology, University of Montenegro, 81000 Podgorica, Montenegro; zeljkoj@ucg.ac.me

* Correspondence: berta.hollo@dh.uns.ac.rs

Abstract: The synthesis of the first Ag(I) complexes with ethyl-5-amino-1-methyl-1H-pyrazole-4-carboxylate (L) is presented. The reaction of AgClO₄ with the ligand in a molar ratio of 1:1 gives a bis(ligand) complex [AgL₂]ClO₄ (1) in the presence of 4-formylbenzotrile, monoperoxypolymer {[AgL₂]ClO₄]_n (2). Characterization involved IR spectroscopy, conductometric measurements, thermogravimetric analysis, antioxidant tests, powder, and single crystal X-ray diffraction. Structural analysis revealed ligand coordination in a monodentate manner through the nitrogen atom of the pyrazole ring in both complexes. Complex 1 displayed a linear coordination environment for Ag(I), whereas, in complex 2, square-planar coordination was achieved with the additional involvement of two oxygen atoms from bridging perchlorate anions. Notably, the thermal properties of both isomers are found to be nearly identical. The significant antioxidant activity of the isomer with a reverse-oriented pyrazole-type ligand suggests its potential relevance in biological studies.

Keywords: pyrazole derivatives; silver complexes; structural analysis; thermal analysis; antioxidant activity



Citation: Radnović, N.D.; Štetin, N.; Radanović, M.M.; Borišev, I.Đ.; Rodić, M.V.; Jaćimović, Ž.K.; Barta Holló, B. Two Isomers of a Novel Ag(I) Complex with Pyrazole-Type Ligand—Synthesis, Structural, Thermal, and Antioxidative Characterization. *Inorganics* **2024**, *12*, 4. <https://doi.org/10.3390/inorganics12010004>

Academic Editor: László Kótai

Received: 24 November 2023

Revised: 12 December 2023

Accepted: 14 December 2023

Published: 21 December 2023



Copyright: © 2023 by the authors. Licensee MDPI, Basel, Switzerland. This article is an open access article distributed under the terms and conditions of the Creative Commons Attribution (CC BY) license (<https://creativecommons.org/licenses/by/4.0/>).

1. Introduction

Pyrazole derivatives are used in different fields due to the aromatic character of the pyrazole ring. Their metal complexes are also the focus of different studies and development activities in preparing new materials with better photophysical, magnetic, or even pharmaceutical activities. In the literature, complex compounds of pyrazole derivatives with good photoluminescence [1] and good magnetic properties [1–3] can be found. Bi- and tri-functional derivatives may be used to prepare 1D–3D coordination polymers, enlarging the field of possible applications of coordination compounds with pyrazole-type ligands [4–6]. On the other hand, numerous pyrazoles and their complexes show significant antimicrobial [7–9], antipyretic [10], anti-inflammatory [11], and even antiproliferative activity [12,13].

Silver(I) compounds are known as good antimicrobial agents [7,14]. The Ag(I) ion can also form coordination polymers with photocatalytic and photoluminescent properties [15,16]. In complex compounds, Ag(I) is often bicoordinated, but in coordination polymers, it forms three or four coordinative bonds. In considering the coordinative and biological properties of silver(I) ions and the good coordination ability of ethyl-5-amino-1-methyl-1H-pyrazole-4-carboxylate (L) and earlier results achieved with it [17,18], our group is focused on research related to L and its coordination complexes.

Since the most economic syntheses are those where product properties can be finely tuned by reaction conditions, the detailed structural and physicochemical characterization of new compounds is crucial for further compound design. Therefore, in this paper, the synthesis, structure, spectral, and thermoanalytical characterization, as well as the antioxidative properties of the two isomers of a silver(I) complex with ethyl-5-amino-1-methyl-1H-pyrazole-4-carboxylate (**L**) and perchlorate, are presented.

2. Results and Discussion

2.1. Compound Syntheses

The reaction between silver perchlorate and ethyl-5-amino-1-methyl-1H-pyrazole-4-carboxylate (**L**) was examined in two solvents, methanol and acetonitrile, to obtain single crystals. It was found that the solvent did not affect the product of the synthesis. These syntheses gave $[\text{AgL}_2]\text{ClO}_4$ (**1**) with pyrazole moieties of the same orientation in either case. Experiments were repeated with the addition of 4-formylbenzotrile to the ligand solution before the addition of AgClO_4 to the reaction mixture. In this case, a monoperoiodic polymer $\{[\text{AgL}_2\text{ClO}_4]\}_n$ (**2**) with reverse-oriented pyrazoles and a perchlorate anion as a bridging ligand was obtained. These results suggest that the solvent does not affect the properties of the product of the synthesis. Despite this, the addition of 4-formylbenzotrile to the ligand solution does not modify the pyrazole-type ligand, nor coordinates to the silver(I) ion, but it changed the orientation of coordinated pyrazole-type ligands. This led us to the conclusion that 4-formylbenzotrile induced different reaction mechanisms and thus has a modulator role.

Molar conductivity values measured in freshly prepared DMF solutions of the compounds show that their solutions are electrolytes 1:1 type [19]. It suggests that **1** dissociated to $[\text{AgL}_2]^+$ and ClO_4^- ions. Although **2** also dissociates to $[\text{AgL}_2]^+$ and ClO_4^- ions, in the last complex cation, pyrazole moieties are reverse-oriented, which is a significant difference compared to the complex cation of **1**. It might play a role in the differences between the antioxidative activities of compounds **1** and **2**. On the other hand, the slightly different values of molar conductivity may suggest the slightly different mobility of two different complex cations, which also suggests that the two cations have different physicochemical and/or biological properties. These results are in accordance with the crystal structure of **1**, which proves the ionic nature of the perchlorate ion in **1** and the expected low stability of monoperoiodic polymer **2** in solution. Since the compounds crystallize in the form of single crystals, their molecular and crystal structures are determined by X-ray diffraction.

2.2. Crystal and Molecular Structure

The molecular structure of **1** (Figure 1a) consists of an Ag^+ , two **L** in their neutral form, and a perchlorate ion. Silver atom is situated in a linear environment, composed of two ligands that are coordinated in a monodentate manner through the nitrogen atoms N1A and N1B, respectively. Angle N1A–Ag1–N1B value of $174.05(8)^\circ$ shows deformation from an ideal angle of 180° for linear geometry, which can be explained by electrostatic attraction of Ag1 towards O1C (the closest oxygen atom from the perchlorate anion) with an $\text{Ag}\cdots\text{O1C}$ distance of $2.907(14)$ Å. Coordination bond lengths for Ag1–N1A and Ag1–N1B were $2.111(2)$ and $2.1116(19)$ Å, respectively, which were in accordance with values found in structures containing fragments of the type $\text{Ag}-\text{N}(\text{pz})_2$ (CSD refcodes: ISAHUH [20], JAXKOL [21], UNONER [22], and ZULJUN [23]). Both pyrazole rings of **L** show a high level of planarity and the dihedral angle between those rings is $4.04(12)^\circ$.

The asymmetric unit of **2** is constituted by half a unit each of Ag^+ and perchlorate ion, situated in special positions, and one unit of **L**. Silver ion occupies a special position with site symmetry $\bar{1}$ (inversion center) while a chlorine atom occupies a special position with site symmetry 2 (two-fold rotation axis). The organic ligand is coordinated in the same way as observed in **1**. In contrast to the weaker coordination ability of the perchlorate anion, the distance between Ag1 and O1C ($2.778(4)$ Å) in **2** is shorter than the distance between Ag1 and O1C found in **1** and can be considered as a coordination bond. Additionally,

the Ag–O1C distance in **2** is comparable to those observed in structures with a square-planar $\text{AgN}_2(\text{ClO}_4)_2$ fragment (CSD refcodes: LITBAT ($d = 2.798 \text{ \AA}$) [24] and CEZPUU ($d = 2.819 \text{ \AA}$) [25]). Therefore, in **2** perchlorate anion acts as bidentate coligand and had a bridging role connecting two silver atoms through O1C atoms, forming a monoperiodic polymer (Figure 2b). This rearrangement of atoms resulted in Ag^+ ions situated in a square planar environment. Because N donor atoms of the ligand are inversion related, the angle N1–Ag1–N1(ii) has an ideal value of 180° while N1–Ag1–O1C and N1(ii)–Ag1–O1C have values of $94.51(11)^\circ$ and $85.49(11)^\circ$, respectively, forming perfectly planar geometry.

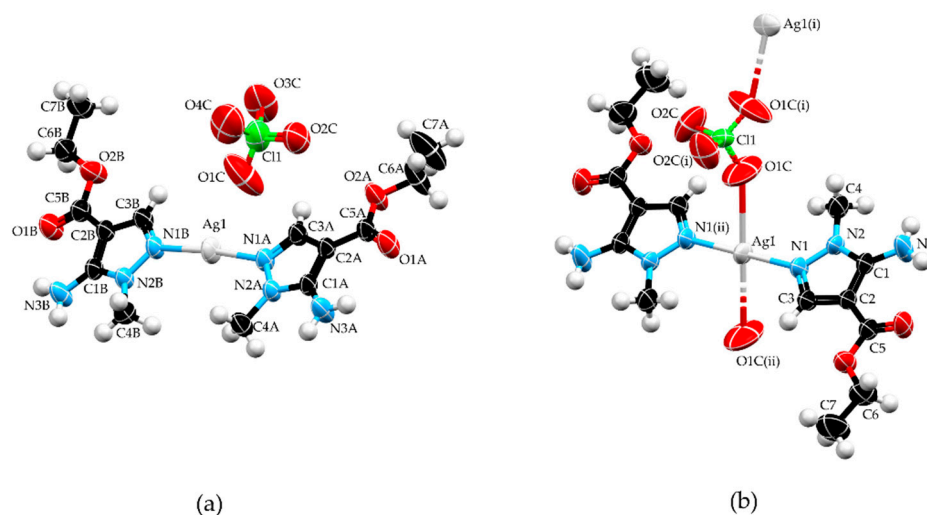


Figure 1. Molecular structures of complexes **1** (a) and **2** (b). Symmetry operations: (i) $-x, y, 1/2 - z$; (ii) $-x, -y, -z$. Color code: silver—light gray, carbon—black, nitrogen—blue, oxygen—red, chlorine—green, and hydrogen—white.

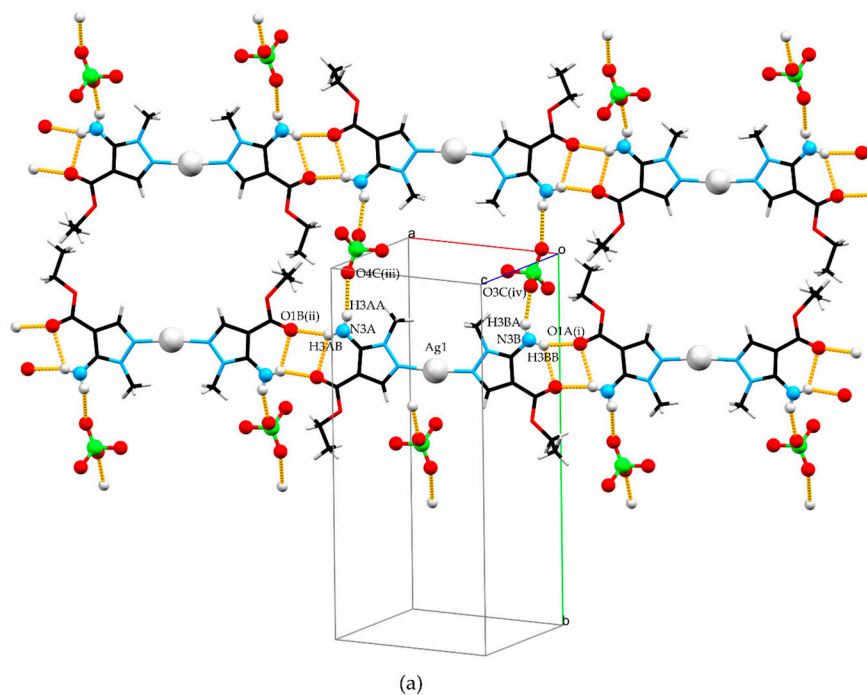


Figure 2. Cont.

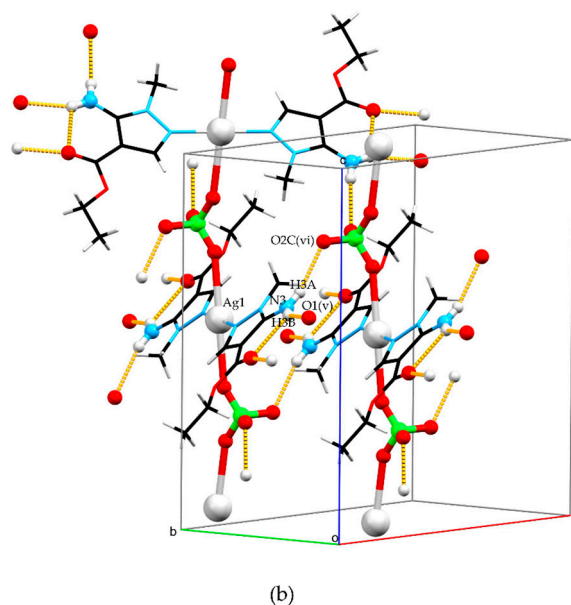


Figure 2. Crystal structures of complexes **1** (a) and **2** (b). A capped sticks model was used to increase the visibility of crystal packing while a Ball and Stick model was used to emphasize donors and acceptors of hydrogen bonds and perchlorate anion roles in packing. Color code: silver—light gray, carbon—black, nitrogen—blue, oxygen—red, chlorine—green, and hydrogen—white.

The electrostatic attraction of complex cations and perchlorate anions is dominant in structure **1** (Figure 2a), but there is also N–H···O hydrogen bonding that additionally stabilizes the crystal structure. The coordinated ligand in **1** forms the chain that extends along the crystallographic [3 0 1] direction via N3A–H3AB···O1B(i) and N3B–H3BB···O1A(ii) hydrogen bonds while a perchlorate ion interconnects two chains via N3A–H3AA···O4C(iii) and N3B–H3BA···O3C(iv) hydrogen bonds. Additionally, two intramolecular N3A–H3AB···O1A and N3B–H3BB···O1B hydrogen bonds are present in **L**, both between amine and carbonyl groups of the ester fragment. Table 1 lists all geometry parameters of the hydrogen bonds present in complexes **1** and **2**.

Table 1. Hydrogen bonding geometry parameters for complexes **1** and **2**.

Bond	Distances, Å			Angles, °	Symmetry Operation on A
	D–H	H···A	D···A	D–H···A	
1					
N3A–H3AB···O1B(i)	0.84(2)	2.24(2)	3.019(3)	163 (3)	$-x + 3/2, y - 1/2, -z + 3/2$
N3B–H3BB···O1A(ii)	0.84(2)	2.20(2)	2.990(3)	170 (3)	$-x + 3/2, y - 1/2, -z + 3/2$
N3A–H3AA···O4C(iii)	0.84(2)	2.43(2)	3.247(8)	126 (3)	
N3B–H3BA···O3C(iv)	0.81(2)	2.18(2)	2.963(6)	155 (3)	$x + 3/2, -y + 1/2, z + 1/2$
N3A–H3AB···O1A	0.84(2)	2.39(3)	2.956(3)	162 (4)	$x - 1/2, -y + 1/2, z - 1/2$
N3B–H3BB···O1B	0.84(2)	2.36(3)	2.894(3)	157 (3)	$x - 3/2, -y + 1/2, z - 1/2$
N3A–H3AA···O1D(v)	0.84(2)	2.34(2)	3.170(12)	123 (3)	
2					
N3–H3B···O1(v)	0.84(2)	2.14(3)	2.903(3)	124 (4)	$-x + 1, y - 1, -z + 3/2$
N3–H3A···O2C(vi)	0.84(2)	2.28(2)	3.107(4)	151 (4)	$-x + 1/2, -y - 1/2, -z + 1$

Polymeric chains of **2** propagate along crystallographic axis *c* (Figure 2b). Those chains are interconnected in two ways by hydrogen bonding. One is through a N3–H3B···O1(v) hydrogen bond which results in the formation of a chain extending along the crystallographic [1 3 0] direction. This chain connects coordinated ligand molecules in a similar way to structure **1**.

The second way of interconnecting two polymeric chains is through an N3–H3A···O2C(vi) hydrogen bond which also shows the second role of the perchlorate anion as a hydrogen bond

acceptor, besides its primary role bridging two silver atoms. This way of packing results in the formation of a complex three-periodic network consisting of covalent and hydrogen bonds.

To check the phase purity of complexes, powder X-ray diffraction (PXRD) patterns of bulk samples of **1** and **2** were recorded at room temperature. Results are presented in Figures 3 and 4, together with simulated diffractograms derived from crystal structures. A near-perfect agreement was observed in diffractograms for complex **2**, indicating excellent phase purity of the compound. Conversely, the diffractogram of **1** exhibited additional peaks corresponding to an unidentified phase, implying the possible presence of unreacted species. This observation lends support to the idea that the inclusion of 4-formylbenzointrile in the reaction mixture during the synthesis of complex **2** contributes to an enhanced crystallinity in the final product. It further confirms the aforementioned hypothesis that this compound acts as a modulator in the process.

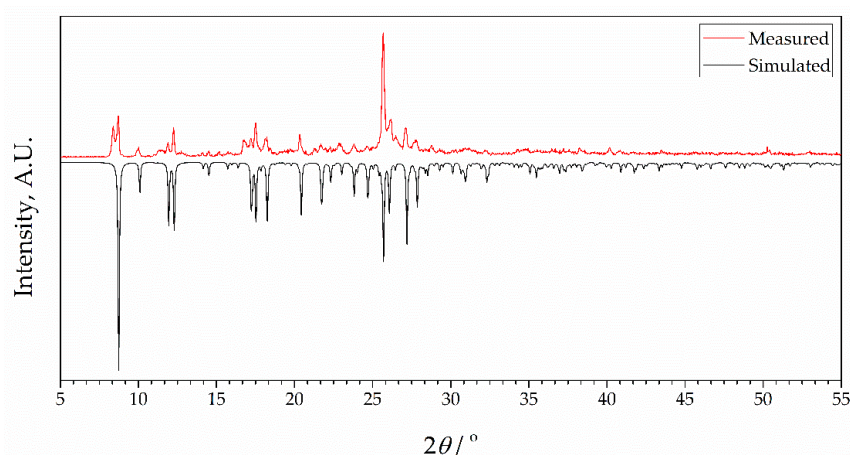


Figure 3. X-ray powder diffraction data for complex **1** showing patterns simulated from single crystal data at 273 K (black) and measured as synthesized (red, room temperature). Intensities of simulated data are inverted for ease of comparison.

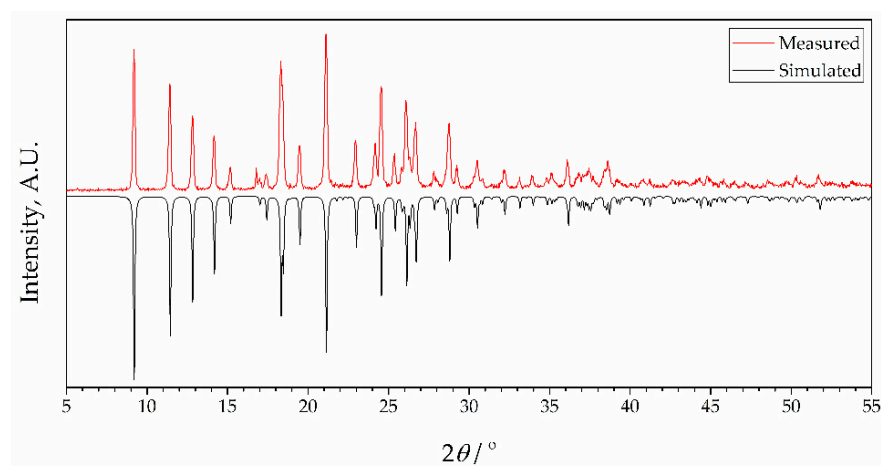


Figure 4. X-ray powder diffraction data for complex **2** showing patterns simulated from single crystal data at 273 K (black) and measured as synthesized (red, room temperature). Intensities of simulated data are inverted for ease of comparison.

2.3. IR Spectra of L, **1**, and **2**

The IR spectra of **1** and **2**, compared to the spectrum of the pure ligand show some differences (Figure 5). Since **L** is coordinated as a monodentate through the free N atom of the pyrazolic ring, differences between spectra are small and mostly result from different interactions in the crystal lattice of the new compounds. The most significant changes are observed between 3500 and 2800 cm^{-1} in the region of O–H, N–H, and C–H vibrations.

The free ligand has bands between 3300 and 3100 cm^{-1} , while in the spectra of **1** and **2** instead of them two partially overlapped strong bands somewhat above 3300 cm^{-1} are observed. Differently, the strong bands in the range 1700–1500 cm^{-1} in the spectra of the complexes are shifted toward lower wavenumbers compared to the spectrum of the **L**. Differences can be observed in the range 1300–1200 cm^{-1} also. Below 1200 cm^{-1} the bands of the ligand are shifted toward lower wavenumbers, but also the characteristic wide band of the perchlorate appears at $\sim 1100 \text{ cm}^{-1}$, thus it cannot be assigned with certainty. The main reason for this is that the wavenumbers of the split bands of ClO_4^- are very close to each other, and if some other bands, e.g., bands of organic ligands are detected at close wavenumbers, they are overlapping and difficult to assign split bands. Thus, the small band detected at 1123 cm^{-1} , which looks like a result of splitting, can not with certainty be assigned to it because of the overlapping with the intensive bands of the ligand at 1125 and 1110 cm^{-1} . It looks like the splitting of perchlorate, due to coordination, is not enough to separate into a triplet as can be expected due to the coordination of the perchlorate ion [26]. However, a similar situation was found in other silver perchlorate complexes [27–29]. On the other hand, the splitting of the characteristic perchlorate band at $\sim 620 \text{ cm}^{-1}$ may prove the different nature of the perchlorate group [30]. In the spectrum of **1**, one intensive band at 619 cm^{-1} is detected, while in the spectrum of **2**, two bands at 622 and 603 cm^{-1} were identified. In this range (below 700 cm^{-1}), the spectra of the complexes are also different compared to the same range in the IR spectrum for **L**.

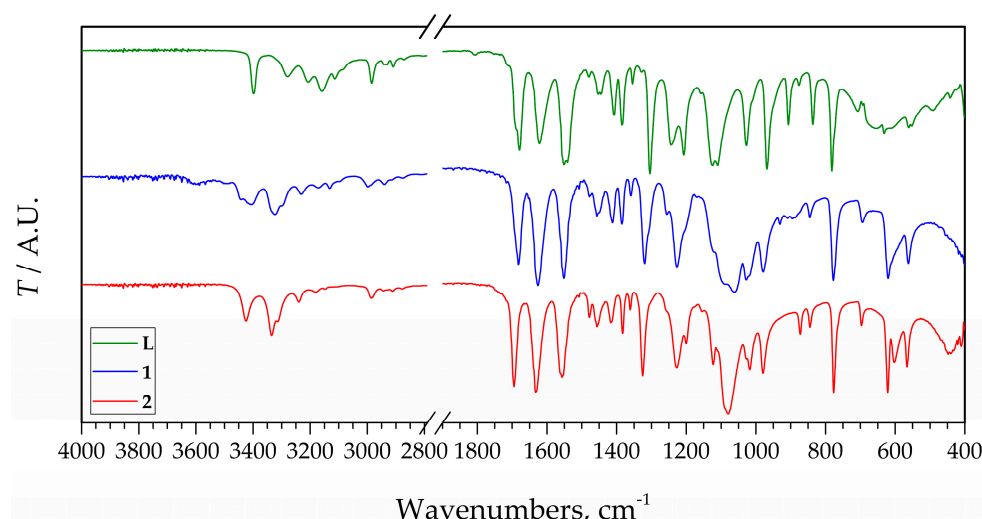


Figure 5. IR spectra for **L** and compounds **1** and **2**.

2.4. Thermal Properties

For complexes **1** and **2**, with the same composition but differently oriented pyrazole moieties, it was interesting to determine if the orientation of the ligand affects the thermal properties of the compound, and if the polymer is more stable than the monomer complex. With this aim, measurements were carried out in both inert and oxidizing atmospheres. Firstly, a pre-experiment was performed in an inert atmosphere to determine the safest conditions for measurements considering the perchlorate content of **1** and **2**. Both complexes were analyzed in nitrogen (Figure 6). Up to $\sim 270 \text{ }^\circ\text{C}$, the only significant difference between thermal curves (TG DTG, and DSC) is that **1** contains some solvent, most probably absorbed moisture, which evaporates somewhat above room temperature. This evaporation results in a mass loss of 0.4% and finished up to $60 \text{ }^\circ\text{C}$. Compound **2** does not contain an absorbed solvent. Both compounds are stable up to relatively high temperatures. DTG curves suggest that above $180 \text{ }^\circ\text{C}$, compound **1** begins to decompose in overlapped processes, but the differences in DTG and TG curves between **1** and **2** are very small. Above $200 \text{ }^\circ\text{C}$, two partially overlapped DTG peaks are detected in both cases with maximums of 238 and 266 for **1** and 235 and 268 for **2**, respectively. In this step, **1** lost 40.1% of its mass, but

this step does not finish before the beginning of the next step, in which the mass loss is 11.6%. In the case of **2**, these two steps overlapped more, therefore the overall mass loss was determined as 59.2% up to 400 °C. These mass loss steps may be correlated to the partial decomposition of pyrazole-type ligands (62.01% for two **L** molecules) and the decomposition of perchlorate. Above this temperature, one more step is observed in both cases, in which **1** loses 8.4% while **2** lost 10.7%. DTG maximums were 450 and 447 °C for **1** and **2**, respectively.

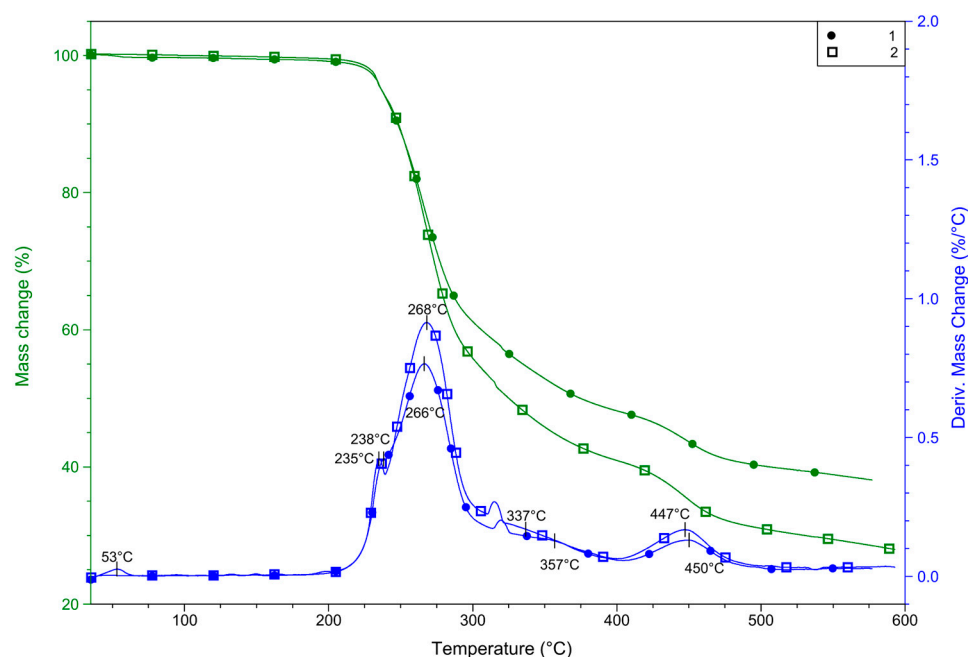


Figure 6. TG and DTG curves for **1** and **2** were recorded in nitrogen.

DSC curves (Figure 7) support the supposed decomposition. The beginning is endothermic, which is in accordance with the decomposition of the organic part of the complex. The sharp endothermic peak also suggests that the complex melts at the beginning of the decomposition. On the other hand, the endothermic peak turns into overlapped exothermic peaks above 260 °C. This exothermic effect suggests that perchlorate, which may easily generate the explosion of the compound, decomposes between 260 and 380 °C. The very low endothermic peaks at 453 °C for **1** and 451 °C for **2** suggest that during the decomposition process, AgCl also forms and melts at 455 °C [31].

Online coupled TG-MS measurements showed that the slight mass loss from room temperature is a water loss process with peaks of 17 and 18 m/z , characteristic for water MS spectrum [32]. This result suggests that compound **1** slightly absorbs moisture from the atmosphere during storage. The intensive peaks at ~300 °C (Figure 8) prove that occurs the oxidative degradation of pyrazole-type ligands. Due to the presence of perchlorate, oxidation in an inert atmosphere is also possible and gives the characteristic fragments of oxidative decomposition of the organic fragments of the compound: 14 m/z for N^+ or CH_2^+ , 16 m/z for O^+ or NH_2^+ , 17 and 18 m/z are together characteristic for H_2O^+ , besides, 17 also partially corresponds to NH_3^+ too [32]. The 29 fragment m/z most probably corresponds to NCH_3^+ or $CH_3CH_2^+$, 36 m/z is usually the mass value of molecular ion HCl^+ , which would prove redox reactions between perchlorate and **L**, but also may correspond to the C_3^+ fragment of the organic ligand. The mass value 44 m/z may have corresponded to two different fragments, CO_2^+ or N_2O^+ , which are both possible to get by oxidation of the pyrazole moiety.

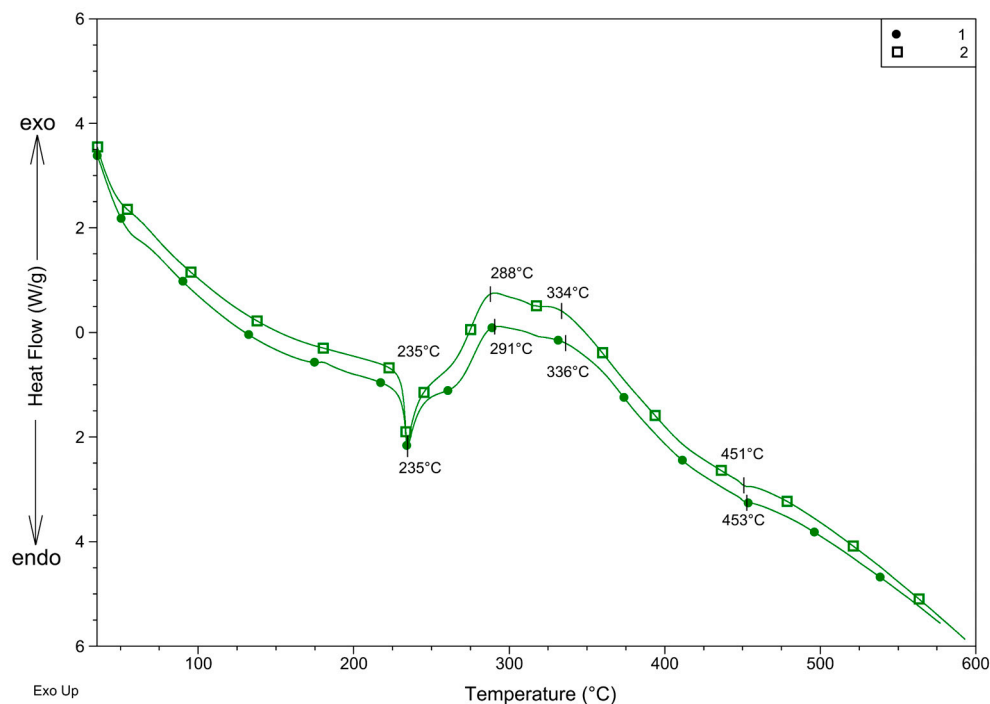


Figure 7. DSC curves of 1 and 2 recorded in nitrogen.

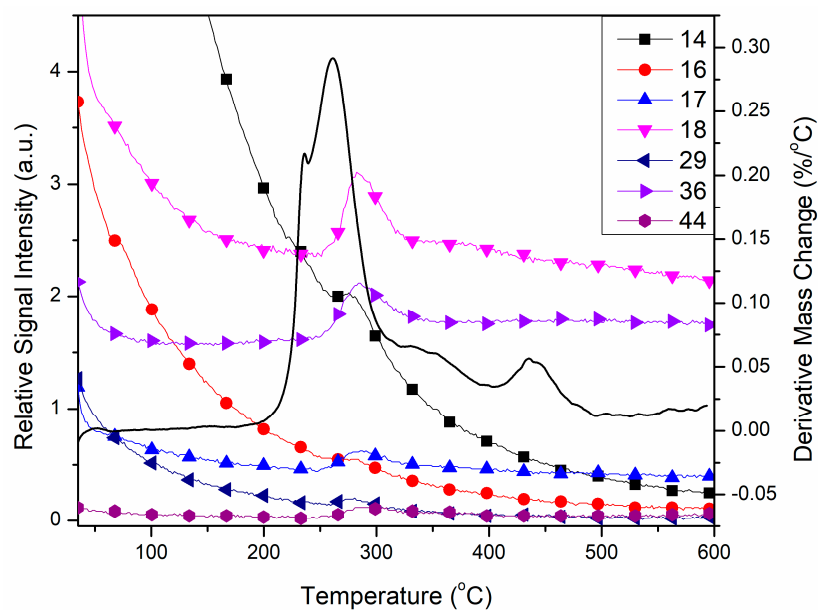


Figure 8. Characteristic fragments of 1 found by TG-MS measurements in argon.

2.5. Antioxidative Properties

Following that, the used pyrazole derivative gave complexes with zinc(II), and some of them showed significant antioxidative capacity, it was interesting to analyze the complexes formed by ethyl-5-amino-1-methyl-1H-pyrazole-4-carboxylate (L) and silver(I) ions to investigate the potential antioxidative properties. Considering that silver is very often biologically active, the effect of the formation of new complexes of Ag(I) with L on the antioxidative capacity of L by 2,2-diphenyl-1-picrylhydrazyl (DPPH) assay was determined.

As presented in Figure 9, the antioxidative capacity of the pyrazole-type ligand is 257.76 μg Trolox equivalent per g of the dry sample mass. It is in range with the earlier determined antioxidative capacity of Zn complexes with L [18]. Compound 1, with pyrazole moieties oriented in the same way, shows somewhat lower activity than that of L (195.53 μg

ek. TE/g.s.m), but polymer **2**, with reverse-oriented pyrazole ligands, shows significantly higher antioxidative activity, 330.60 μg ek. TE/g.s.m. Considering the almost identical molar conductivity of compounds in *N,N*-dimethylformamide (DMF), they are most probably dissociated in the same way in both DMF and DMSO, used in antioxidative tests. Thus, in solution, the most probable ions are ClO_4^- and $[\text{AgL}_2]^+$ and the most significant difference between **1** and **2** is the orientation of L in their cations. Based on our earlier results [18], we concluded that most probably, the amino substituent of the pyrazole ring neutralizes the DPPH• radical. Taking it into account, most probably, differently oriented pyrazole rings in the complexes' structure result in different hindrances and interactions of this group in the solutions of the compounds, therefore, in different free radical scavenging capacities.

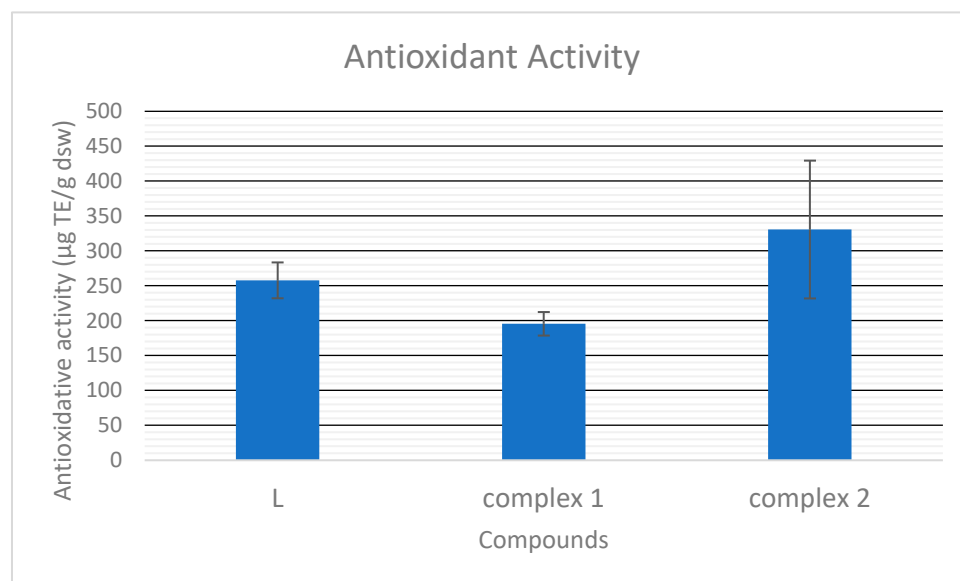


Figure 9. The antioxidative capacity of L and complexes 1 and 2.

3. Materials and Methods

Caution! Perchlorate compounds are potentially explosive; thus, they have to be handled with great care. All chemicals were commercial products and used without further purification.

3.1. Synthesis of $[\text{AgL}_2]\text{ClO}_4$ (**1**) with Same-Oriented Pyrazole-Type Ligands

The solution of the ligand (0.5 mmol, 0.085 g) dissolved in 5 cm^3 acetonitrile was mixed with the solution of AgClO_4 (0.25 mmol, 0.052 mg) in 5 cm^3 acetonitrile. The mixture was shortly heated and covered with aluminum foil. After two days rod-like transparent single crystals were filtered. The synthesis was repeated in methanol and the same product was obtained. Yield: 0.075 g (55%). Molar conductivity ($\lambda_{\text{M}}(\text{DMF})$) 82.7 $\text{S cm}^2 \text{mol}^{-1}$.

3.2. Synthesis of $\{[\text{AgL}_2]\text{ClO}_4\}_n$ (**2**) with Reverse-Oriented Pyrazole-Type Ligands

The mixture of the ligand (0.5 mmol, 0.085 g) and 4-formylbenzotrile (0.5 mmol, 0.069 g) was dissolved in 10 cm^3 methanol and refluxed for 2 h. The reaction mixture became yellowish. After the reflux was finished, AgClO_4 (0.5 mmol, 0.113 mg) was added to the reaction mixture, and all that was shortly heated, then covered with aluminum foil. After three days transparent prismatic single crystals with rose shine were filtered. Yield: 0.090 g (33%). Molar conductivity ($\lambda_{\text{M}}(\text{DMF})$) 79.6 $\text{S cm}^2 \text{mol}^{-1}$.

3.3. Analytical Techniques

IR spectra were recorded on a Thermo Nicolet iS20 FTIR spectrophotometer (Thermo Fisher Scientific, Waltham, MA, USA) with Smart iTR™ ATR Sampling accessories, in the range of 4000–400 cm^{-1} . Molar conductivities of freshly prepared complex solutions

($c = 1 \times 10^{-3} \text{ mol dm}^{-3}$) were measured on a Jenway 4510 conductivity meter. Thermal data were collected by measurements on a TA Instruments SDT Q600 thermal analyzer in the range from room temperature to 600 °C at 10 °C min⁻¹ heating rate in nitrogen (flow rate = 100 cm³·min⁻¹). Sample holder/reference: alumina crucible/empty alumina crucible. Sample mass 2.5–3 mg. The TG-MS data were collected on the same thermal instrument, coupled to the Hiden Analytical HPR20/QIC mass spectrometer. The analyses were carried out in the range from room temperature to 600 °C at 10 °C min⁻¹ heating rate in argon (flow rate = 50 cm³·min⁻¹). Selected ions between $m/z = 1$ –81 were monitored in multiple ion detection mode (MID).

3.4. Crystal Structure Determination

Crystallographic and refinement details are listed in Table 2. All data were collected at room temperature. CrysAlisPro8 [33] was used for instrument control and data reduction. Crystal structures were solved using the iterative dual-space routine in SHELXT [34] and refined with SHELXL [35]. All non-hydrogen atoms were refined anisotropically, while hydrogen atoms were placed in idealized positions and refined using a riding model.

Table 2. Crystallographic and refinement details.

	1	2
<i>Crystal data</i>		
Chemical formula	C ₁₄ H ₂₂ AgClN ₆ O ₈	C ₁₄ H ₂₂ AgClN ₆ O ₈
M_r	545.69	545.69
Crystal system	Monoclinic	Monoclinic
Space group	<i>P</i> 2 ₁ / <i>n</i>	<i>C</i> 2/ <i>c</i>
$a/\text{Å}$	9.96262 (16)	19.2386 (6)
$b/\text{Å}$	20.2514 (4)	7.3795 (2)
$c/\text{Å}$	10.5085 (3)	15.4908 (5)
$\alpha/^\circ$	90	90
$\beta/^\circ$	102.5209 (19)	93.943 (3)
$\gamma/^\circ$	90	90
$V/\text{Å}^3$	2069.74 (7)	2194.03 (12)
Z	4	4
Radiation type	Mo $K\alpha$	Mo $K\alpha$
μ/mm^{-1}	1.16	1.09
Crystal size, mm	0.39 × 0.32 × 0.19	0.48 × 0.23 × 0.18
<i>Data collection</i>		
Absorption correction	Analytical	Analytical
T_{min}	0.724	0.685
T_{max}	0.829	0.860
Measured reflections	27,536	12,513
Independent reflections	5183	2718
Observed reflections [$I > 2\sigma(I)$]	3761	2173
R_{int}	0.031	0.043
$(\sin \theta / \lambda)_{\text{max}}/\text{Å}^{-1}$	0.628	0.625
<i>Refinement</i>		
$R [F^2 > 2\sigma(F^2)]$	0.036	0.039
$wR [F^2]$	0.096	0.103
S	1.02	1.06
Reflections	5183	2718
Parameters	345	148
H-atom treatment	Mixed	Mixed
$\Delta\rho_{\text{max}}/e \text{ Å}^{-3}$	0.43	0.45
$\Delta\rho_{\text{min}}/e \text{ Å}^{-3}$	−0.55	−0.39

The final structures underwent internal validation using PLATON [36] and external validation using the Cambridge Structural Database (CSD) [37] via MOGUL [38] knowledge bases, accessible through Mercury CSD [39].

Powder X-ray diffraction (PXRD) measurements were performed on a Rigaku Miniflex 600 (U = 40 kV, I = 15 mA, Cu K α radiation λ = 0.15406 nm) instrument using a counting step of 0.03° and counting time per step of 3 s. All samples were mounted on a zero-background silicon sample holder and measured at room temperature in the 2 θ range of 5–55°. Obtained data were compared against simulated patterns from single crystal data collections at 295 K.

3.5. Determination of DPPH• Radical Neutralization Capability

The synthesized samples were tested for scavenging effect on the DPPH radical (DPPH) according to a slightly modified method by Soler-Rivas et al. [40]. The method is based on the spectrophotometric monitoring of the transformation of the violet-colored, stable, nitrogen-centered DPPH• radical (2,2-diphenyl-1-picrylhydrazyl) into the reduced, yellow-colored form of DPPH-H. The DPPH• radical is a relatively stable radical whose solution in methanol is purple with an absorption maximum at λ_{\max} = 515 nm. The presence of potential electron donors or H atoms leads to the neutralization of DPPH radicals and transition to a neutral form, which is followed by a change in absorbance and the disappearance of the purple color of the solution. The tested samples were dissolved in 15% DMSO in methanol (15% v/v) solution, and a series of concentrations (ranging from 10 to 40 mg/mL) were prepared. The solutions have been tested using 96-well microplates. Fifty microliters of the sample's solution were added to the 160 microliters of DPPH solution (previously prepared as a 0.4 mmol/l solution in 96% ethanol, which was then diluted four times in methanol to give an absorbance at 515 nm of 0.9) and 90 microliters of methanol were added to reach the final volume of 300 μ L. Blank (the tested sample is substituted with the used solvent) and matrix blank (solvent and samples without DPPH solution) probes have also been added. At the same time, the series of Trolox solutions (ranging from 1 to 100 mg/mL) for the calibration curve were prepared. The DPPH solution and methanol were added to the Trolox samples in the same amounts as the tested samples. Absorbance at 515 nm was measured after 60 min. The antioxidant activity is expressed as micrograms of Trolox equivalents per gram of dry samples weight (μ g TE/g dsw).

4. Conclusions

The reaction of AgClO $_4$ and the ligand, ethyl-5-amino-1-methyl-1H-pyrazole-4-carboxylate (L) resulted in the formation of a new silver(I) complex with the formula [AgL $_2$]ClO $_4$. In this complex, two pyrazole-type ligands are coordinated in the same orientation (1). When the same reaction was performed in the presence of 4-formyl benzonitrile, the monoperiodic polymer (2) was obtained, with the reverse-orientation of the pyrazole-type ligands. The thermoanalytical measurements showed that differently oriented pyrazole moieties and polymerization do not affect thermal properties nor compound stability. However, antioxidant activity is significantly better in the case of complex 2, i.e., the polymer with the reverse orientation of two L molecules.

Author Contributions: Conceptualization, B.B.H., M.V.R. and M.M.R.; methodology, N.D.R. and B.B.H.; investigation, N.Š., N.D.R., I.Đ.B. and B.B.H.; resources, Ž.K.J.; writing—original draft preparation, M.M.R. and N.D.R.; writing—review and editing, M.V.R., M.M.R. and B.B.H.; visualization, N.D.R.; supervision, M.V.R., M.M.R. and B.B.H.; funding acquisition, B.B.H. and Ž.K.J. All authors have read and agreed to the published version of the manuscript.

Funding: This research was funded by the Ministry of Science, Technological Development and Innovation of the Republic of Serbia (Grant No. 451-03-47/2023-01/200125).

Data Availability Statement: Crystallographic data associated with this publication are deposited with the Cambridge Crystallographic Data Centre under the CCDC Numbers 2309974–2309975. They are freely available at <https://www.ccdc.cam.ac.uk/structures>.

Acknowledgments: The authors are grateful to Srđan Rakić for PXRD measurements.

Conflicts of Interest: Author Nađa Štetin was employed by the company Telix d.o.o. The remaining authors declare that the research was conducted in the absence of any commercial or financial relationships that could be construed as a potential conflict of interest.

References

1. Lavrenova, L.G.; Ivanova, A.D.; Bogomyakov, A.S.; Smolentsev, A.I.; Burdukov, A.B.; Sheludyakova, L.A.; Vasilevskii, S.F. Cobalt(II), Nickel(II), and Copper(II) Bromide Complexes with 3-Amino-4-Ethoxycarbonylpyrazole: Syntheses, Structures, and Magnetic Properties. *Russ. J. Coord. Chem./Koord. Khimiya* **2015**, *41*, 86–92. [[CrossRef](#)]
2. Shakirova, O.G.; Korotaev, E.V.; Petrov, S.A.; Varnek, V.A.; Lavrenova, L.G. Spin Crossover in Iron(II) Complexes with Tris(Pyrazol-1-Yl)Methane and [Ag(CN)₂]- and [Au(CN)₂]- Anions. *J. Struct. Chem.* **2022**, *63*, 1538–1550. [[CrossRef](#)]
3. Berezin, A.S.; Komarovskikh, A.Y.; Komarov, V.Y.; Syrovkashin, M.M.; Sheven, D.G. Trinuclear Copper(II) Bromide Complex [C₃H₅N₃Br]₂: N[Cu₃Br₈]_n. Structure, Magnetic Properties and DFT Calculations. *New J. Chem.* **2019**, *43*, 18203–18209. [[CrossRef](#)]
4. Berezin, A.S.; Nadolinny, V.A.; Lavrenova, L.G. Synthesis, Structure, and Properties of a Copper Bromide Coordination Compound with 3-Amino-4-EthoxyCarbonylPyrazole. Nature of the Nonresonant and Ferromagnetic Absorption Observed by EPR. *J. Supercond Nov. Magn.* **2015**, *28*, 1007–1011. [[CrossRef](#)]
5. Berezin, A.S.; Ivanova, A.D.; Komarov, V.Y.; Nadolinny, V.A.; Lavrenova, L.G. Influence of Water on the Structure and Magnetic Properties of a Copper Bromide Coordination Compound with 3-Amino-4-Ethoxycarbonylpyrazole. *New J. Chem.* **2018**, *42*, 4902–4908. [[CrossRef](#)]
6. Netto, A.V.G.; Frem, R.C.G.; Mauro, A.E.; Crespi, M.S.; Zorel, H.E. Synthesis, Spectral and Thermal Studies on Pyrazolate-Bridged Palladium(II) Coordination Polymers. *J. Therm. Anal. Calorim.* **2007**, *87*, 789–792. [[CrossRef](#)]
7. Matiadis, D.; Karagiaouri, M.; Mavroidi, B.; Nowak, K.E.; Katsipis, G.; Pelecanou, M.; Pantazaki, A.; Sagnou, M. Synthesis and Antimicrobial Evaluation of a Pyrazoline-Pyridine Silver(I) Complex: DNA-Interaction and Anti-Biofilm Activity. *BioMetals* **2021**, *34*, 67–85. [[CrossRef](#)]
8. Patil, P.; Yadav, A.; Bavkar, L.; Nippu, B.N.; Satyanarayan, N.D.; Mane, A.; Gurav, A.; Hangirgekar, S.; Sankpal, S. [MerDABCO-SO₃H]Cl Catalyzed Synthesis, Antimicrobial and Antioxidant Evaluation and Molecular Docking Study of Pyrazolopyranopyrimidines. *J. Mol. Struct.* **2021**, *1242*, 130672. [[CrossRef](#)]
9. Soliman, S.M.; Almarhoon, Z.; Sholkamy, E.N.; El-Faham, A. Bis-Pyrazolyl-s-Triazine Ni(II) Pincer Complexes as Selective Gram Positive Antibacterial Agents; Synthesis, Structural and Antimicrobial Studies. *J. Mol. Struct.* **2019**, *1195*, 315–322. [[CrossRef](#)]
10. Badaweya, E.-S.A.M.; El-Ashmaweyb, I.M. Nonsteroidal Antiinflammatory Agents-Part 1: Antiinflammatory, Analgesic and Antipyretic Activity of Some New 1-(Pyrimidin-2-Yl)-3-Pyrazolin-5ones and 2-(Pyrimidin-2-Yl)-1,2,4,5,6,7-Hexahydro-3H-Indazol-3-Ones. *Eur. J. Med. Chem.* **1998**, *33*, 349–361. [[CrossRef](#)]
11. Gökhan-Keleşçi, N.; Yabanoğlu, S.; Küpeli, E.; Salgin, U.; Özgen, Ö.; Uçar, G.; Yeşilada, E.; Kendi, E.; Yeşilada, A.; Bilgin, A.A. A New Therapeutic Approach in Alzheimer Disease: Some Novel Pyrazole Derivatives as Dual MAO-B Inhibitors and Antiinflammatory Analgesics. *Bioorg. Med. Chem.* **2007**, *15*, 5775–5786. [[CrossRef](#)] [[PubMed](#)]
12. Barra, C.V.; Rocha, F.V.; Netto, A.V.G.; Frem, R.C.G.; Mauro, A.E.; Carlos, I.Z.; Ananias, S.R.; Quilles, M.B. New Palladium(II) Complexes with Pyrazole Ligands: Part II. Synthesis, Spectral and Thermal Studies, and Antitumor Evaluation. *J. Therm. Anal. Calorim.* **2011**, *106*, 483–488. [[CrossRef](#)]
13. de Andrade Querino, A.L.; Enes, K.B.; Chaves, O.A.; Dittz, D.; Couri, M.R.C.; Diniz, R.; Silva, H. Modified Pyrazole Platinum(II) Complex Can Circumvent Albumin and Glutathione: Synthesis, Structure and Cytotoxic Activity. *Bioorg Chem.* **2020**, *100*, 103936. [[CrossRef](#)]
14. Santos, A.F.; Ferreira, I.P.; Pinheiro, C.B.; Takahashi, J.A.; Teixeira, L.R.; Beraldo, H. Silver(I) Complexes with 2,6-Diacetylpyridine-Bis(Benzoylhydrazones): Antifungal Activity and Interaction with DNA. *Polyhedron* **2017**, *138*, 270–276. [[CrossRef](#)]
15. Ristić, P.; Filipović, N.; Blagojević, V.; Ćirković, J.; Barta Holló, B.; Đokić, V.R.; Donnard, M.; Gulea, M.; Marjanović, I.; Klisurić, O.R.; et al. 2D and 3D Silver-Based Coordination Polymers with Thiomorpholine-4-Carbonitrile and Piperazine-1,4-Dicarbonitrile: Structure, Intermolecular Interactions, Photocatalysis, and Thermal Behavior. *CrystEngComm* **2021**, *23*, 4799–4815. [[CrossRef](#)]
16. Ristić, P.; Todorović, T.R.; Blagojević, V.; Klisurić, O.R.; Marjanović, I.; Barta Holló, B.; Vulić, P.; Gulea, M.; Donnard, M.; Monge, M.; et al. 1D and 2D Silver-Based Coordination Polymers with Thiomorpholine-4-Carbonitrile and Aromatic Polyoxoacids as Coligands: Structure, Photocatalysis, Photoluminescence, and TD-DFT Study. *Cryst. Growth Des.* **2020**, *20*, 4461–4478. [[CrossRef](#)]
17. Barta Holló, B.; Vojinović Ješić, L.S.; Radanović, M.M.; Rodić, M.V.; Jaćimović, Ž.K.; Mészáros Szécsényi, K. Synthesis, Physicochemical, and Thermal Characterization of Coordination Compounds of Cu(II) with a Pyrazole-Type Ligand. *J. Therm. Anal. Calorim.* **2020**, *142*, 451–460. [[CrossRef](#)]
18. Barta Holló, B.; Radanović, M.M.; Rodić, M.V.; Krstić, S.; Jaćimović, Ž.K.; Vojinović Ješić, L.S. Synthesis, Physicochemical, Thermal and Antioxidative Properties of Zn(II) Coordination Compounds with Pyrazole-Type Ligand. *Inorganics* **2022**, *10*, 20. [[CrossRef](#)]
19. Geary, W.J. The Use of Conductivity Measurements in Organic Solvents for the Characterisation of Coordination Compounds. *Coord. Chem. Rev.* **1971**, *7*, 81–122. [[CrossRef](#)]
20. Guo, Q.; Englert, U. An Acetylacetonate or a Pyrazole? Both! 3-(3,5-Dimethyl-Pyrazol-4-Yl)Pentane-2,4-Dione as a Ditopic Ligand. *Cryst. Growth Des.* **2016**, *16*, 5127–5135. [[CrossRef](#)]
21. Amolegbe, S.A.; Akinremi, C.A.; Adewuyi, S.; Lawal, A.; Bamigboye, M.O.; Obaleye, J.A. Some Nontoxic Metal-Based Drugs for Selected Prevalent Tropical Pathogenic Diseases. *J. Biol. Inorg. Chem.* **2017**, *22*, 1–18. [[CrossRef](#)] [[PubMed](#)]

22. Crawford, D.; Hofer, A.K.; Edler, K.L.; Ferrence, G.M. Bis(3,5-Dimethyl-1H-Pyrazole-KN2)Silver(I) Hexafluoroantimonate. *Acta Crystallogr. Sect. E Struct. Rep. Online* **2011**, *67*, m496. [[CrossRef](#)] [[PubMed](#)]
23. Tian, A.; Ning, Y.; Yang, Y.; Hou, X.; Ying, J.; Liu, G.; Zhang, J.; Wang, X. Three New POM-Based Compounds Constructed by Rigid Thiabendazole and Flexible Bis(Pyrazole) Ligands: Structures and Properties for Hg²⁺ Recognition. *Dalton Trans.* **2015**, *44*, 16486–16493. [[CrossRef](#)] [[PubMed](#)]
24. Garai, M.; Biradha, K. Coordination Polymers of Organic Polymers Synthesized via Photopolymerization of Single Crystals: Two-Dimensional Hydrogen Bonding Layers with Amazing Shock Absorbing Nature. *Chem. Commun.* **2014**, *50*, 3568–3570. [[CrossRef](#)] [[PubMed](#)]
25. Zhang, Z.Y.; Deng, Z.P.; Huo, L.H.; Zhao, H.; Gao, S. Anion-Assisted Silver(I) Coordination Complexes from Flexible Unsymmetrical Bis(Pyridyl) Ligands: Syntheses, Structures and Luminescent Properties. *Polyhedron* **2013**, *59*, 38–47. [[CrossRef](#)]
26. May, N.V.; Bayat, N.; Béres, K.A.; Bombicz, P.; Petruševski, V.M.; Lendvay, G.; Farkas, A.; Kótai, L. Structure and Vibrational Spectra of Pyridine Solvated Solid Bis(Pyridine)Silver(I) Perchlorate, [Agpy₂ClO₄]_{0.5}py. *Inorganics* **2022**, *10*, 123. [[CrossRef](#)]
27. Lissner, F.; Hartenbach, I.; Schleid, T. K₃Er₇S₁₂ Und Rb₃Er₇S₁₂: Zwei Ternäre Erbium(III)-Sulfide Mit Kanalstruktur. *Z Anorg. Allg. Chem.* **2002**, *628*, 1552–1555. [[CrossRef](#)]
28. Franguelli, F.P.; Béres, K.A.; Kótai, L. Pyridinesilver Tetraoxometallate Complexes: Overview of the Synthesis, Structure, and Properties of Pyridine Complexed AgxO₄ (x = Cl, Mn, Re) Compounds. *Inorganics* **2021**, *9*, 79. [[CrossRef](#)]
29. Fogaça, L.A.; Bereczki, L.; Petruševski, V.M.; Barta-Holló, B.; Franguelli, F.P.; Mohai, M.; Béres, K.A.; Sajó, I.E.; Szilágyi, I.M.; Kótai, L. A Quasi-Intramolecular Solid-Phase Redox Reaction of Ammonia Ligands and Perchlorate Anion in Diamminesilver(I) Perchlorate. *Inorganics* **2021**, *9*, 38. [[CrossRef](#)]
30. Lewis, D.L.; Estes, E.D.; Hodgson, D.J. The Infrared Spectra of Coordinated Perchlorates. *J. Cryst. Mol. Struct.* **1975**, *5*, 67–74. [[CrossRef](#)]
31. Greenwood, N.N.; Earnshaw, A. *Chemistry of the Elements*; Elsevier B.; Elsevier Butterworth-Heinemann: Oxford, UK, 1997; ISBN 0 7506 3365 4.
32. Welcome to the NIST WebBook. Available online: <https://webbook.nist.gov/> (accessed on 1 October 2021).
33. Rigaku Oxford. *Diffraction CrystAlisPro Software System*; Rigaku Corporation: Wroclaw, Poland, 2019.
34. Sheldrick, G.M. Foundations and Advances SHELXT-Integrated Space-Group and Crystal-Structure Determination. *Acta Crystallographica Section A* **2015**, *71*, 3–8. [[CrossRef](#)]
35. Sheldrick, G.M. Crystal Structure Refinement with SHELXL. *Acta Crystallogr. Sect. C* **2015**, *C71*, 3–8. [[CrossRef](#)]
36. Spek, A.L. Structure Validation in Chemical Crystallography. *Acta Crystallogr. D Biol. Crystallogr.* **2009**, *65*, 148–155. [[CrossRef](#)] [[PubMed](#)]
37. Groom, C.R.; Bruno, I.J.; Lightfoot, M.P.; Ward, S.C. The Cambridge Structural Database. *Acta Crystallogr. B Struct. Sci. Cryst. Eng. Mater.* **2016**, *72*, 171–179. [[CrossRef](#)] [[PubMed](#)]
38. Bruno, I.J.; Cole, J.C.; Kessler, M.; Luo, J.; Momerwell, W.D.S.; Purkis, L.H.; Smith, B.R.; Taylor, R.; Cooper, R.I.; Harris, S.E.; et al. Retrieval of Crystallographically-Derived Molecular Geometry Information. *J. Chem. Inf. Comput. Sci.* **2004**, *44*, 2133–2144. [[CrossRef](#)]
39. MacRae, C.F.; Sovago, I.; Cottrell, S.J.; Galek, P.T.A.; McCabe, P.; Pidcock, E.; Platings, M.; Shields, G.P.; Stevens, J.S.; Towler, M.; et al. Mercury 4.0: From Visualization to Analysis, Design and Prediction. *J. Appl. Crystallogr.* **2020**, *53*, 226–235. [[CrossRef](#)]
40. Soler-Rivas, C.; Espín, J.C.; Wichers, H.J. An Easy and Fast Test to Compare Total Free Radical Scavenger Capacity of Foodstuffs. *Phytochem. Anal.* **2000**, *11*, 330–338. [[CrossRef](#)]

Disclaimer/Publisher's Note: The statements, opinions and data contained in all publications are solely those of the individual author(s) and contributor(s) and not of MDPI and/or the editor(s). MDPI and/or the editor(s) disclaim responsibility for any injury to people or property resulting from any ideas, methods, instructions or products referred to in the content.